Journal of Applied Polymer Science

Approach to the fabrication of acrylic elastomer nanocomposites with high dielectric constants

Jie Wang, Jing-Wen Wang, Shu-Wei Zhou, Gao-Qiang Wang, Su Zhang
Department of Materials Science and Engineering, College of Materials Science and Technology, Nanjing University of Aeronautics and Astronautics, Nanjing 211106, People's Republic of China
Correspondence to: J.-W. Wang (E-mail: wjw_msc@nuaa.edu.cn)

ABSTRACT: Dielectric elastomers (DEs) are a type of electroactive polymer that can deform in an electric field. The possession of a high dielectric constant is critical for DEs if they are to be suitable materials for the application of actuators. A novel elastomeric nanocomposite (ACE-*g*-CuPc) was fabricated by copper phthalocyanine oligomer (CuPc) grafting directly onto an acrylic elastomer (ACE) backbone. Compared with other synthetic methods, esterification has several advantages; these include fewer impurities and a simpler synthetic route. Transmission electron microscopy showed that the size of the CuPc particles of the ACE-*g*-CuPc was in the range 15–30 nm; this range was significantly smaller than that of ACE/CuPc (500 nm). The results of thermogravimetric analysis show that the thermal stability of the grafting composite was higher than that of the blending composite. At 100 Hz, the dielectric constant of the grafting composite (with 11 wt % CuPc) reached 173 at room temperature. © 2016 Wiley Periodicals, Inc. J. Appl. Polym. Sci. **2016**, *133*, 43904.

KEYWORDS: composites; dielectric properties; elastomers; films; grafting

Received 25 December 2015; accepted 8 May 2016
DOI: 10.1002/app.43904

INTRODUCTION

Recently, much attention has been paid to dielectric elastomers (DEs) in the field of novel actuators. DEs are a type of electroactive polymer that can deform in an electric field; thereby, they generate stress and convert electrical energy into mechanical energy.[1,2] DEs have several impressive advantages, including a low cost, large deformation, short response time, and light weight.[3] Thus, DEs are desirable candidates for the application of actuators.[4,5] The DE actuator is composed of a DE film coated with compliant electrodes on the both sides of the film. When a driving voltage is applied, the film decreases in thickness and expands in area. When the driving voltage disappears, the film returns to its initial status.[6–9]

Silicones, polyurethane, and acrylic elastomer (ACE) are the most widely used DEs.[10] Compared with silicones and polyurethane, ACE can yield extremely large strains.[11] In this research, styrene, butyl acrylate, and hydroxyethyl acrylate were selected as monomers to synthesize ACE with hydroxyl groups by free-radical copolymerization. The strain of ACE is influenced by the electric field intensity and the dielectric constant. In a low electric field, the large strain of DE could be realized with an increasing dielectric constant. The reliability and security for practical applications can be improved as the driving electric field decreases. Consequently, the possession of a high dielectric constant is critical for DEs as suitable materials for the application of actuators.

In recent years, numerous methods have been tried to increase the dielectric constant of DEs. The method of adding various high-dielectric-constant fillers (inorganic and/or organometallic) into DEs has made great progress.[12–15] Compared with inorganic fillers, organometallic fillers show excellent flexibility and low elastic modulus values. Copper phthalocyanine oligomer (CuPc; Figure 1) is a type of organometallic filler that exhibits an extremely high dielectric constant ($>10^5$).[16]

However, in a blended composite, CuPc fillers prefer to agglomerate because of the incompatibility between CuPc and the matrix; this decreases the dielectric constant and breakdown field of the composite. To solve this problem, the formation of chemical bonds between the matrix and the filler to reduce the size of CuPc particles is a viable method. According to the exchange coupling effect, the dielectric constant of a composite will be improved when the size of CuPc particles is reduced. Liu *et al.*[17] reported a nanocomposite of ACE with CuPc. In that research, they introduced isocyanate groups onto the ACE chain with toluene diisocyanate (TDI) reacting with ACE; this facilitated the grafting of CuPc with —COOHs onto the backbone of the chemically modified ACE. However, the method was not convenient because of the complicated synthesis procedure,

low reproducibility, pollution, and long reaction time. Moreover, it was difficult to control the reaction products of the grafting reaction through Liu's method. For example, because of the fact that the isocyanate groups of TDI could react with both carboxyl groups and hydroxyl groups, two ACE chains could react with the same TDI monomer. Moreover, two hydroxyl groups of one ACE chain could also react with the same TDI monomer. Thus, some TDI monomers could not play a role in the grating of CuPc fillers onto the ACE matrix. Consequently, a simple, reproducible, and scalable grafting procedure is still needed. In this research, CuPc fillers were directly grafted onto the ACE matrix.

EXPERIMENTAL

Materials

The synthetic route of the CuPc oligomer was reported in ref. 18. Styrene and butyl acrylate were purified with a sodium hydroxide solution and distilled before use. To remove inhibitors, hydroxyethyl acrylate was purified with activated carbons. Benzoyl peroxide was recrystallized from methanol before use. Dimethylformamide (DMF) was purified with CaH_2 and distilled before use. Dicyclohexylcarbodiimide (DCC) and 4-dimethylaminopyridine (DMAP) were analytical grade and were used without further purification.

Synthesis of ACE-*g*-CuPc

The synthetic route of the grafting composite was as follows. A 100-mL, three-necked, round-bottomed flask was used as the reactor. Butyl acrylate (0.65 g), styrene (0.30 g), hydroxyethyl acrylate (0.05 g), and DMF (1 mL) were added to the reactor sequentially. Then, a DMF solution (0.2 mL) with benzoyl peroxide (0.0056 g) was added to the reactor. The reaction mixture was magnetically stirred for 5 h at 100 °C and then cooled to 25 °C. A calculated amount of a CuPc/DMF solution (4 mL) was activated with DMAP (0.0053 g) and DCC (0.0977 g) and was then added to the reactor. Next, the reaction system was kept at a temperature of 25 °C for 24 h. The impurities were removed by filtration, and DMF was eliminated by vacuum distillation.

Preparation of the Composite Films

The composite films were prepared by a solution casting method. For the ACE-*g*-CuPc film, ACE-*g*-CuPc was added to DMF. After the ACE-*g*-CuPc was fully dissolved in DMF, the solution was poured into a polytetrafluoroethylene mold and kept at 120 °C for 10 h. Next, the composite was annealed at 120 °C *in vacuo* for 12 h. For the physical blending of the composite of ACE and CuPc oligomer (ACE/CuPc), ACE and CuPc were fully dissolved in DMF; then, the compound was exposed to ultrasound until the ACE and CuPc were uniformly mixed. The later procedure was the same as that used for the preparation of the ACE-*g*-CuPc film.

Instrumentation

The IR spectrum was recorded by a Nicolet Nexus-670 with KBr as the background. With chloroform-*d* as the solvent, the ^{1}H-NMR spectrum was recorded with a Bruker DRX-500. Inductively coupled plasma atomic emission spectrometry was performed with a Jarrell-Ash J-A1100. The curves of differential scanning calorimetry (DSC) were collected by a PerkinElmer DSC Pyris 1. The curves of thermogravimetric analysis (TGA) were recorded with a Netzsch TGA 409PC calorimeter. Samples (10–12 mg) were sealed in Al_2O_3 pans, and the temperature was measured from 25 to 600 °C at a rate of 10 °C/min. The morphology of the composites was collected by transmission electron microscopy (TEM; JEM-100S). The curves of X-ray diffraction (XRD) were collected by a Bruker D8 Advance rotating anode X-ray generator. The films were cut into small pieces with dimensions of 10 × 10 mm^2, and the angle was measured from 10 to 50° at a rate of 10°/min.[19] The dielectric properties were recorded with an HP 4294A impedance analyzer. The films were cut into small pieces with dimensions of 5 × 5 mm^2, and circular carbon grease electrodes 3 mm in diameter were coated in the center on both sides of each sample. The dielectric constants of the samples were calculated with a parallel-plate capacitor equation:

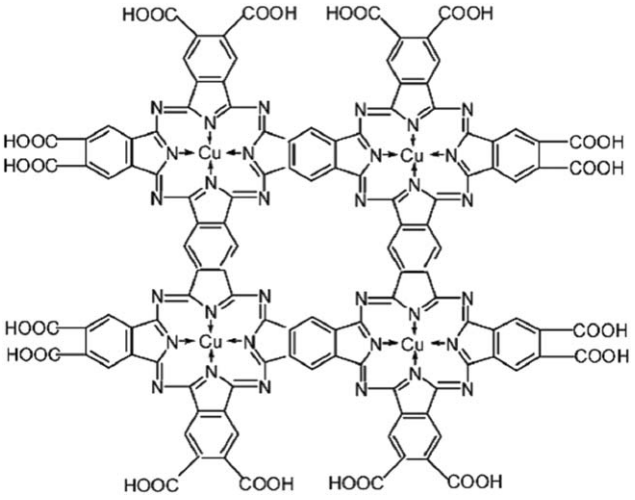

Figure 1. Chemical structure of the CuPc oligomer.

$$\text{Dielectric constant} = \frac{Ch}{\varepsilon_0 A} \quad (1)$$

where C is the capacitance, h is the thickness of the film, ε_0 is the vacuum dielectric permittivity, and A is the area of the electrode. The elastic modulus of the film was measured by a dynamic mechanical thermal analyzer (DMTA-V). The testing mode was the strain rate mode, and the frequency was 1 Hz.

RESULTS AND DISCUSSION

Synthesis of ACE-*g*-CuPc

In this research, DCC and DMAP were selected as the water absorbent and catalyst, respectively. The carboxyl group reacted more easily with the hydroxyl groups of DCC and DMAP.[20,21] Thereby, the CuPc molecules were grafted onto the ACE backbone directly with the method of esterification. Figure 2 shows the Fourier transform infrared spectra of ACE and ACE-*g*-CuPc. The characteristic peaks of ACE at 1028, 1260, 1452, 1494, 2957, and 3028 cm^{-1} appeared in the ACE-*g*-CuPc spectrum, too. The characteristic peak appearing at 1718 cm^{-1} was intrinsic to the stretching vibrations of the carbonyl groups of —COO— in the spectrum of ACE; however, the corresponding peak appeared at 1708 cm^{-1} in the spectrum of ACE-*g*-CuPc. The esterification of hydroxyl groups in ACE-*g*-CuPc caused newly generated ester groups. Compared with the ester groups

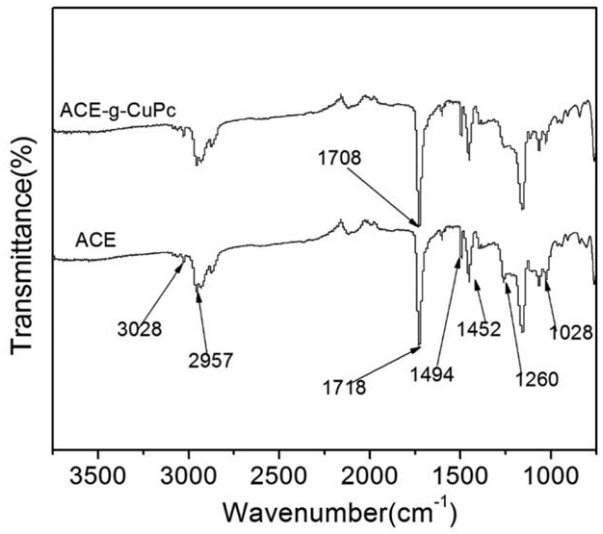

Figure 2. Fourier transform infrared spectra of ACE and ACE-*g*-CuPc.

of ACE, the carbon atoms of the newly generated ester groups connected to the benzene ring instead of to the alkyl; thus, the characteristic peak moved to the right.[22]

Figure 3 shows the ^{1}H-NMR spectra of ACE/CuPc and ACE-*g*-CuPc. At 4.81 ppm, the characteristic peak in the spectrum of ACE indicated the hydrogen of —O**H**, which vanished in the spectrum of ACE-*g*-CuPc. The chemical shift value of the hydrogen of —C**H**$_2$—O— appeared at 3.60 ppm in the spectrum of ACE; however, the corresponding peak appeared at 3.81 ppm in the spectrum of ACE-*g*-CuPc. The chemical shift value was determined by the electron cloud density of hydrogen nuclei, and the chemical shift value decreased when the electron cloud density increased. Because the electron absorption ability of the ester groups was stronger than that of the hydroxyl groups, the esterification of the partial hydroxyl groups in ACE-*g*-CuPc led the electron density of the hydrogen atom of —C**H**$_2$—O— to decrease. As a result, the chemical shift value increased.[23] The phenomenon verified that the grafting reaction was successful.

According to the inductively coupled plasma atomic emission spectrometry analysis, we calculated that after the esterification, 93.7% of the CuPc oligomers were successfully grafted onto the ACE backbone.

Microstructure of the Composites

The TEM micrographs of ACE/CuPc and ACE-*g*-CuPc are shown in Figure 4. It was obvious that the fillers were aggregated into particles in both composite samples. For ACE-*g*-CuPc, because the CuPc oligomer was grafted onto the ACE backbone, the compatibility was better. Thus, smaller sized particles were observed in ACE-*g*-CuPc. The size of the CuPc particles of the ACE-*g*-CuPc was in the range 15–30 nm; this was significantly smaller than that of ACE/CuPc (500 nm).

Figure 5 shows the XRD curves of ACE, ACE/CuPc, and ACE-*g*-CuPc. The amorphous structure of ACE led to the characteristic peak appearing at 2θ (20.9°) in both samples. Because of the existence of CuPc molecules, the ordered structure of the ACE molecule in the composites was disturbed. Consequently, the diffraction peak intensity appearing at 20.9° was sharply weakened. Because of the (021) plane reflection of the CuPc structure, the characteristic peak appeared at 26.7° in both composites. In ACE/CuPc, the movement of the CuPc molecules was easier than those in ACE-*g*-CuPc. Thus, the crystallization degree of CuPc was higher. Accordingly, the characteristic peak of the ACE-*g*-CuPc was lower than that of the ACE/CuPc at 26.7°. According to the Scherrer equation, the calculated grain size of the composite (L_{021}) was 8.98 nm:

$$L_{hkl} = \frac{0.89\lambda}{B\cos\theta} \quad (2)$$

where L_{hkl} is the grain size, λ is the wavelength of the X-ray, B is the full width at half-maximum of the diffraction peak at 2θ, and θ is the peak angular position.

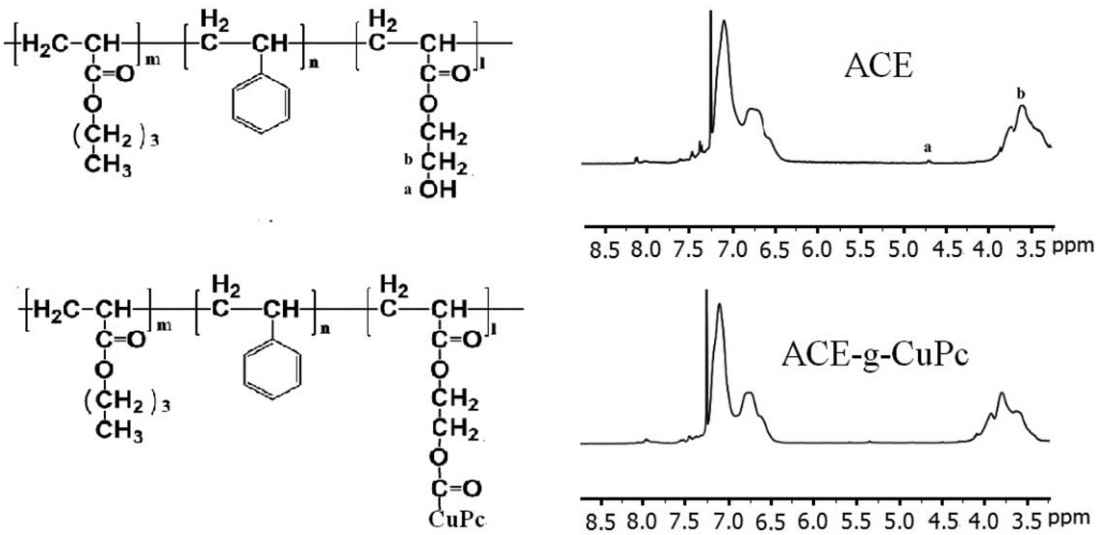

Figure 3. ^{1}H-NMR spectra of ACE and ACE-*g*-CuPc.

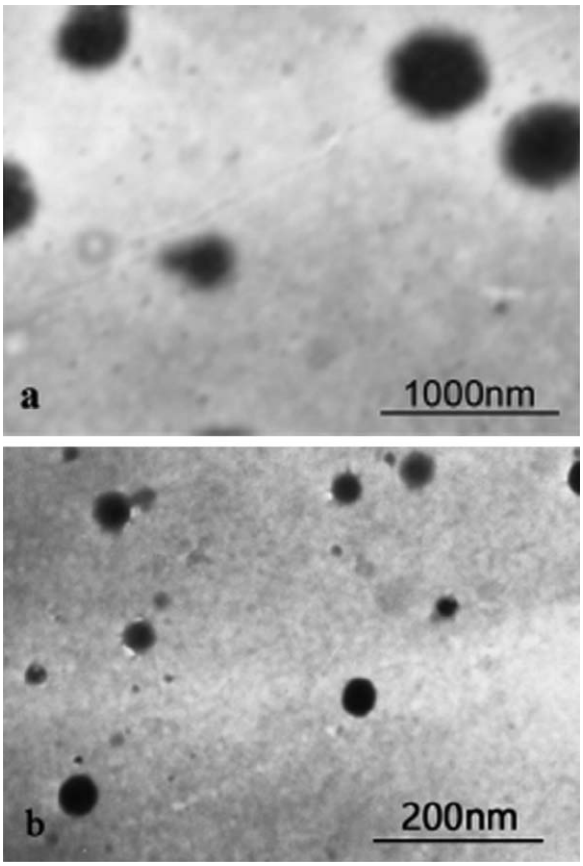

Figure 4. TEM photographs of (a) ACE/CuPc and (b) ACE-*g*-CuPc. The CuPc content in both composites was 11 wt %.

Thermal Behavior of ACE and ACE-*g*-CuPc

Figure 6 shows the DSC curves of the ACE and ACE-*g*-CuPc. In ACE, the corresponding values of the decomposition enthalpy (ΔH_d) and decomposition temperature were 536.7 J/g and 413.2 °C, respectively. In ACE-*g*-CuPc, the values of ΔH_d and the decomposition temperature were 493.2 J/g and 413.0 °C, respectively. According to ref. 21, the degradation temperature of the filler was at least 660 °C; thus, the decomposition of the composite was actually the decomposition of the matrix. Deducting the content of 11 wt % CuPc in the composite, the value of ΔH_d of ACE was equivalent to 554.2 J/g. It was obvious that the value of ΔH_d of ACE was lower than that of the composite. We concluded that because of the crosslinking effect of the CuPc particles, the thermal stability of ACE-*g*-CuPc was improved.

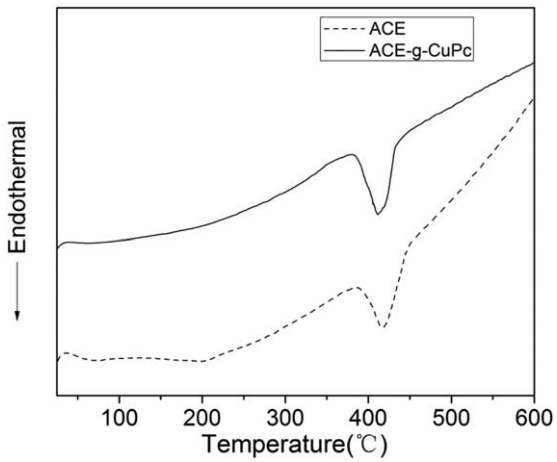

Figure 6. DSC curves of ACE and ACE-*g*-CuPc.

The TGA curves of ACE, ACE/CuPc, and ACE-*g*-CuPc are given in Figure 7. When the temperature ranged from 50 to 300 °C, the curves of the ACE, ACE/CuPc, and ACE-*g*-CuPc descended slightly. This phenomenon was caused by the decomposition of some small molecules. When the temperature ranged from 300 to 600 °C, the weights of ACE, ACE/CuPc, and ACE-*g*-CuPc decreased significantly. In this stage, the decomposition temperatures of ACE, ACE/CuPc, and ACE-*g*-CuPc appeared at 330, 341, and 345 °C, respectively. The decomposition temperatures at 5% of ACE, ACE/CuPc, and ACE-*g*-CuPc appeared at 347, 350, and 359 °C, respectively. The weight losses of the composites were lower than that of ACE (96.6%). The weight loss of the ACE-*g*-CuPc was 80.3%; this was lower than that of ACE/CuPc (82.3%). We concluded that the thermal stability of the grafted composite was improved as a result of it being lightly crosslinked.

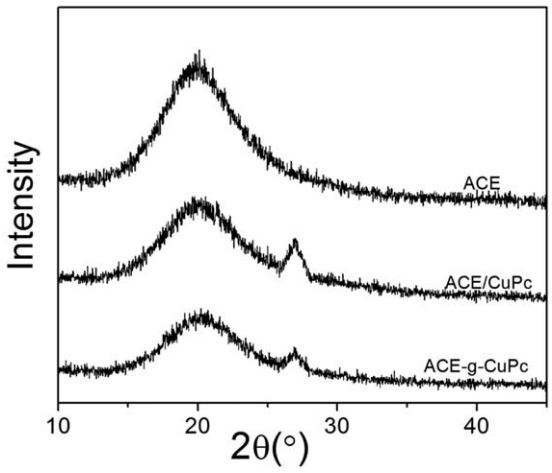

Figure 5. XRD curves of ACE, ACE/CuPc, and ACE-*g*-CuPc. The CuPc content in both composites was 11 wt %.

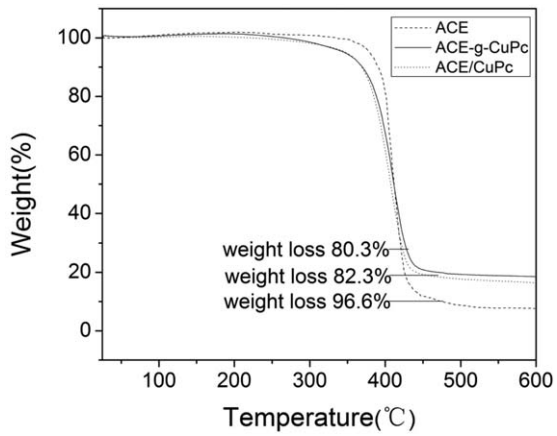

Figure 7. TGA curves of ACE, ACE/CuPc, and ACE-*g*-CuPc. The CuPc content in both composites was 11 wt %.

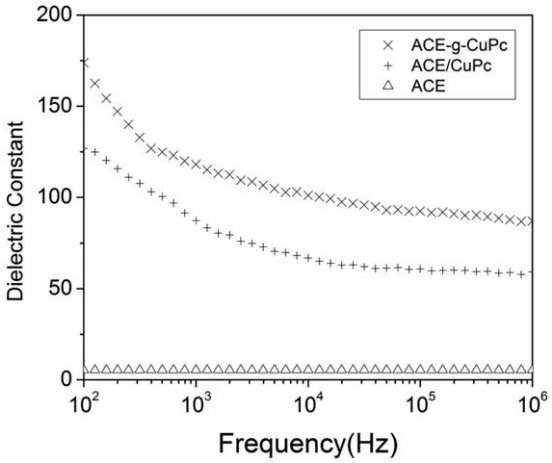

Figure 8. Dielectric constants of ACE, ACE/CuPc, and ACE-*g*-CuPc measured at 25 °C. The CuPc content in both composites was 11 wt %.

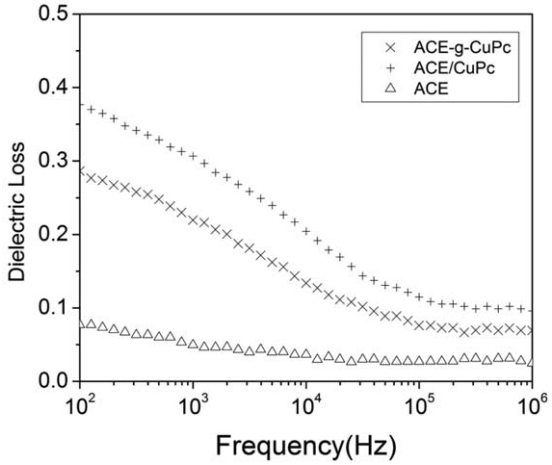

Figure 9. Dielectric losses of ACE, ACE/CuPc, and ACE-*g*-CuPc measured at 25 °C. The CuPc content in both composites was 11 wt %.

Dielectrical Properties of the Composites

Figure 8 shows the dielectric constants of ACE, ACE/CuPc, and ACE-*g*-CuPc (the CuPc contents in both composites were 11 wt %) measured at 25 °C. The dielectric constant of ACE/CuPc was lower than that of ACE-*g*-CuPc. For ACE-*g*-CuPc, as shown in the TEM micrograms, the size of the CuPc particles was smaller than that of ACE/CuPc. Because exchange coupling between the matrix and filler could lead to greatly enhanced polarization in the exchange layer, there was a dramatic enhancement in the dielectric constant of the composites when the size of the CuPc particles decreased.[24]

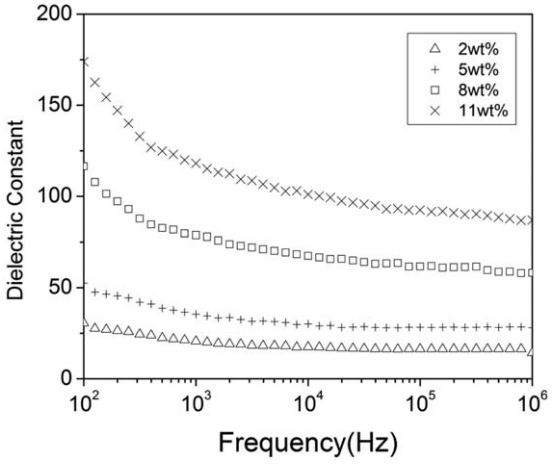

Figure 10. Dielectric constants of ACE-*g*-CuPc measured at 25 °C. The CuPc contents were 2, 5, 8, and 11 wt %.

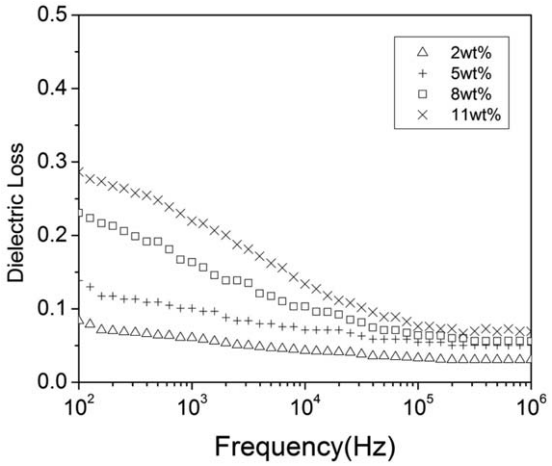

Figure 11. Dielectric losses of ACE-*g*-CuPc measured at 25 °C. The CuPc contents were 2, 5, 8, and 11 wt %.

Figure 9 shows the dielectric losses of ACE, ACE/CuPc, and ACE-*g*-CuPc (the CuPc contents in both composites were 11 wt %) measured at 25 °C. Because the CuPc particles in the grafted composite exhibited excellent dispersibility, it was difficult for the CuPc particles to agglomerate. Over the observed frequency range, the dielectric loss of the ACE-*g*-CuPc was lower than that of ACE/CuPc.

Figures 10 and 11 show the dielectric properties of ACE-*g*-CuPc (the CuPc contents were 2, 5, 8, and 11 wt %, respectively) measured at 25 °C. Over the observed frequency range, the dielectric loss and dielectric constant decreased as the frequency increased. The phenomenon was caused by interfacial polarization, which could be obviously enhanced with increasing content of CuPc. Moreover, the dielectric loss and the dielectric constant increased as the content of CuPc increased. At 100 Hz, the dielectric constant of ACE-*g*-CuPc (the CuPc contents were 2, 5, 8, and 11 wt %, respectively) were 31, 53, 116, and 173, respectively.

ACE-*g*-CuPc not only exhibited good dielectric properties but also showed great flexibility. In this research, the elastic modulus of ACE-*g*-CuPc (the CuPc contents were 2, 5, 8, and 11 wt %, respectively) were 1.03, 1.29, 1.68, and 2.26 MPa, respectively.

CONCLUSIONS

In this research, the novel nanocomposite ACE-*g*-CuPc was fabricated by the grafting of CuPc oligomers onto the ACE backbone with the method of esterification. For ACE-*g*-CuPc, the size of the CuPc particles was in the range 15–30 nm; this was significantly smaller than that of ACE/CuPc (500 nm). The thermal

stability of ACE-*g*-CuPc was higher than that of ACE/CuPc. At 100 Hz, the dielectric constant of the grafting composite (with 11 wt % CuPc) reached 173 at 25 °C.

ACKNOWLEDGMENTS

This work was supported by the National Natural Science Foundation of China (contract grant number 21174063), the Natural Science Foundation of Jiangsu Province (contract grant number BK20131358), the Aeronautical Science Foundation of China (contract grant numbers 2011ZF52063 and 2014ZF52069), and a project funded by the Priority Academic Program Development of Jiangsu Higher Education Institutions.

REFERENCES

1. Carpi, F.; Kornbluh, R.; Sommer-Larsen, P. *Bioinspir. Biomim.* **2011**, *6*, 045006.
2. Jiang, L.; Betts, A.; Kennedy, D. *J. Mater. Sci.* **2015**, *50*, 7930.
3. Suo, Z. *Acta. Mech. Solida. Sin.* **2010**, *23*, 549.
4. Henann, D. L.; Chester, S. A.; Bertoldi, K. *J. Mech. Phys. Solids.* **2013**, *61*, 2047.
5. Plante, J. S.; Dubowsky, S. *Int. J. Solids. Struct.* **2006**, *43*, 7727.
6. Pramanik, B.; Sahu, R. K.; Bhaumik, S. Presented at the IEEE 10th International Conference on the Properties and Applications of Dielectric Materials, Bangalore, India, July **2012**.
7. Kinoshita, Y.; Tsuchitani, S.; Kikuchi, K. Presented at the IEEE/SICE International Symposium on System Integration, Sendai, Japan, December **2010**.
8. Palakodeti, R.; Kessler, M. R. *Mater. Lett.* **2006**, *60*, 3437.
9. Pelrine, R. E.; Kornbluh, R. D.; Joseph, J. P. *Sens. Actuators A.* **1998**, *64*, 77.
10. Zhenyi, M.; Scheinbeim, J. I.; Lee, J. W.; Newman, B. A. *J. Polym. Sci. Part B: Polym. Phys.* **1994**, *32*, 2721.
11. Michel, S.; Zhang, X. Q.; Wissler, M. *Polym. Int.* **2010**, *59*, 391.
12. Wang, J. W.; Wang, Y.; Wang, F. *Polymer* **2009**, *50*, 679.
13. Zhang, Q. M.; Li, H.; Poh, M. *Nature* **2002**, *419*, 284.
14. Bai, Y.; Cheng, Z. Y.; Bharti, V. *Appl. Phys. Lett.* **2000**, *76*, 3804.
15. Wang, J. W.; Shen, Q. D.; Bao, H. M. *Macromolecules* **2005**, *38*, 2247.
16. Wang, J. W.; Wang, Y.; Li, S. Q. *J. Polym. Sci. Part B: Polym. Phys.* **2010**, *48*, 490.
17. Liu, R. N.; Wang, J. W.; Li, Q. *J. Appl. Polym. Sci.* **2014**, *131*, DOI: 10.1002/app.39975.
18. Achar, B. N.; Fohlen, G. M.; Parker, J. A. *J. Polym. Sci. Pol. Chem.* **1982**, *20*, 1785.
19. Tangboriboon, N.; Wongpinthong, P.; Sirivat, A. *Polym. Compos.* **2011**, *32*, 44.
20. Berry, D. J.; DiGiovanna, C. V.; Murugan, R. *Arkivoc* **2001**, *2*, 944.
21. Li, Q. R.; Gu, C. Z.; Yin, H. *Chin. J. Org. Chem.* **2005**, *25*, 1416.
22. Larkin, P. Infrared and Raman Spectroscopy; Principles and Spectral Interpretation; Elsevier: Oxford, United Kingdom, **2011**; Chapter 7, p 124.
23. Silverstein, R. M.; Webster, F. X.; Kiemle, D. Spectrometric Identification of Organic Compounds; Wiley: Hoboken, NJ, **2014**; Chapter 3, p 137.
24. Li, J. Y. *Phys. Rev. Lett.* **2003**, *90*, 217601.